Comparison of the Diagnostic Efficacy of ^{68}Ga-FAPI-04 PET/MRI and ^{18}F-FDG PET/CT in Patients With Pancreatic Cancer

Zeyu Zhang
Changhai Hospital Department of Nuclear Medicine
Guorong Jia
Changhai Hospital Department of Nuclear Medicine
Guixia Pan
Changhai Hospital Department of Nuclear Medicine
Kai Cao
Changhai Hospital Department of Radiology
Qinqin Yang
Changhai Hospital Department of Nuclear Medicine
Hongyu Meng
Shanghai Fourth People's Hospital Department of Radiology
Jian Yang
Changhai Hospital Department of Nuclear Medicine
Lu Zhang
Changhai Hospital Department of Nuclear Medicine
Tao Wang
Changhai Hospital Department of Nuclear Medicine
Chao Cheng (13501925757@163.com)
Changhai Hospital Department of Nuclear Medicine https://orcid.org/0000-0002-2981-5890
Changjing Zuo
Changhai Hospital Department of Nuclear Medicine

Research Article

Keywords: 68Ga-FAPI, 18F-FDG, PET/MR, PET/CT, Pancreatic cancer

Posted Date: September 28th, 2021

DOI: https://doi.org/10.21203/rs.3.rs-922593/v1

Abstract

Purpose

To assess the diagnostic performance of ^{68}Ga-FAPI-04 (^{68}Ga-FAPI) PET/MR for primary as well as metastatic lesions in pancreatic cancer patients and to compare the results with those of ^{18}F-FDG PET/CT.

Methods

Prospectively, we evaluated 31 patients suspected to have pancreatic malignancy. Within one week, each patient underwent both ^{18}F-FDG PET/CT and ^{68}Ga-FAPI PET/MR. Comparisons of the detection abilities and the standardized uptake values (SUVs) for primary tumors, lymph nodes, as well as hepatic metastases were conducted for the two imaging approaches.

Results

Twenty-eight pancreatic cancer patients and three pancreatitis ones were enrolled. ^{68}Ga-FAPI and ^{18}F-FDG exhibited equivalent (100%) detection rates for primary tumors. The SUVs of primary tumors on ^{68}Ga-FAPI PET were markedly higher than those on ^{18}F-FDG ($p < 0.05$). Fifteen pancreatic cancer patients were accompanied by pancreatic parenchymal uptake, whereas ^{18}F-FDG PET images showed parenchymal uptake in 3 patients only (53.57% vs. 10.71%, $p < 0.001$). The number of positive lymph nodes detected was higher for ^{68}Ga-FAPI than for ^{18}F-FDG PET (31 *vs.* 26), led to N upstaging in 27.27% (3/11) of patients, however, the difference was not statistically significant ($p = 0.053$). ^{18}F-FDG PET was able to detect more liver metastases than ^{68}Ga-FAPI, and ^{68}Ga-FAPI uptake of metastatic tumors was significantly lower than ^{18}F-FDG (6.13 ± 1.63 *vs.* 8.09 ± 1.68, $p < 0.001$). In larger liver metastatic lesions, ^{68}Ga-FAPI tended to distribute around the periphery of the lesions. In addition, multiple sequence MR imaging was helpful for finding more micrometastases.

Conclusion

^{68}Ga-FAPI PET demonstrated equivalent detection rate with ^{18}F-FDG for primary tumors of pancreatic cancer, and its percentage of pancreatic parenchymal uptake caused by inflammation was higher. It might be better in the detection of suspicious lymph node metastases. The MR multiple sequence imaging of integrated PET/MR was helpful for detecting tiny liver metastases.

Introduction

Pancreatic cancer is one of the malignancies with high mortality. Its global incidence has tripled since the 1950s, ranking the seventh leading cause of tumor-associated mortalities [1]. Surgical therapy remains the only pancreatic cancer cure. With insidious clinical symptoms, most pancreatic tumors were found at the late stage, causing only 10–20% of patients eligible for surgical resection when detected [2]. Thus,

early pancreatic cancer diagnosis will inform the choice of optimal therapy. Currently, relative to other imaging examinations, positron emission tomography (PET) with ^{18}F-fluorodeoxyglucose (FDG) has higher sensitivity and specificity for pancreatic cancer staging [3,4]. Therapeutic responses and disease recurrence for pancreatic cancer have also been evaluated by ^{18}F-FDG PET/CT [4]. Furthermore, ^{18}F-FDG PET/CT imaging parameters may predict its treatment efficacy and clinical outcome [5]. It should be noted that ^{18}F-FDG sometimes produces false positives for various non-malignant lesions exhibiting a moderate FDG avidity (e.g., reactive lymph nodes or inflammation). And the low resolution of low-dose CT does not allow satisfactory anatomic evaluation of lesions in the retroperitoneal region [6,7].

The combination of PET and magnetic resonance imaging (MRI) is a very capable hybrid imaging technique, which integrates the superiority of MRI soft-tissue contrast with the molecular specificity as well as sensitivity of PET [8]. Integrated PET/MR, as a versatile modality, has the potential to make up for the known limitation of PET/CT in detecting small pancreatic cancer, distinguishing mimics and detecting small hepatic metastases [3,6].

Pancreatic cancer is characterized by a prominent desmoplastic reaction. The desmoplastic stroma is mainly produced by pancreatic stellate cells (PSCs) [9]. Cancer-associated fibroblasts (CAFs) are in part derived from PSCs and transform their tumor-promoting biological properties through crosstalk with neoplastic cells [10,11]. Unlike normal fibroblasts, CAFs in particular play key roles in tumor proliferation, invasion, metastasis, and therapy resistance [12,13]. The expressions of fibroblast activation protein (FAP), an essential homodimeric membrane gelatinase of the dipeptidyl peptidase (DPP) family, in CAFs are selective [14,15]. Based on FAP-specific inhibitors (FAPI), radiopharmaceuticals targeting FAP has been developed. Applications of a ^{68}Ga-labeled FAPI with DOTA-containing ligand (^{68}Ga-FAPI) is a viable radiotracer in detecting malignant cancers; thus, ^{68}Ga-FAPI-based imaging has been important in characterization of various malignant cancers [16,17,18]. Röhrich et al. found that relative to contrast-enhanced CT, ^{68}Ga-FAPI PET/CT is better at detecting recurrent and metastatic lesions in patients with pancreatic ductal carcinoma (PDAC) [18].

This is a prospective study to determine if the performance of ^{68}Ga-FAPI PET/MR is superior to that of ^{18}F-FDG PET/CT in diagnosing primary tumor, involvement of the lymph nodes, as well as distant metastases in patients with pancreatic cancer and to compare the potential impacts of both on therapeutic management.

Materials And Methods

Patients

Thirty-one patients successively diagnosed with suspected pancreatic malignancy by radiologic examinations (contrast-enhanced CT or MRI) were recruited in this study. Patients who were subjected to invasive examinations prior to PET scans, including histopathological biopsy, endoscopic retrograde

cholangiopancreatography (ERCP), and stent placement; received adjuvant radiotherapy or chemotherapy before PET scans; or without available complete clinical or pathological records were excluded. The enrolled patients were subjected to both ^{68}Ga-FAPI PET/MR as well as ^{18}F-FDG PET/CT scans within one week. Prior to their inclusion in this study, all patients signed written informed consents.

Biological and clinical data, including sex, clinical presentation, age, and laboratory indexes were collected from each patient. Final diagnosis was based on the histopathological assessments of tumor samples harvested by surgical resection or biopsy. This prospective study was permitted by the Ethical Committee of the First Affiliated Hospital of Naval Medical University (Changhai Hospital, CHEC2021-071).

Radiopharmaceuticals

Synthesis and labeling of ^{68}Ga-FAPI was according to a previously documented method [19]. ^{68}Ga was obtained from an in-house ^{68}Ge-to-^{68}Ga generator (ITG, Germany). Chelation was done after the adjustment of pH using sodium acetate. Then, for 10 min, heating of the reaction mixture was done to 100 °C for 10 min. The reactions integrity was assessed by radio-liquid chromatography. Solid-phase extraction of ^{68}Ga compounds was performed before injection. The final product was sterile and pyrogen-free.

^{18}F-FDG injections were obtained from Shanghai Atom Kexing Pharmaceutical Co., Ltd. (their radiochemical purity was> 95%).

^{68}Ga-FAPI PET/MR imaging

PET/MR assessments were conducted on an integrated PET/MR scanner (Biograph mMR; Siemens Healthcare, Erlangen, Germany) that has a combination of PET and 3.0-T MRI scanners. Intravenous injection activity of ^{68}Ga-FAPI was 1.85–3.70 MBq/kg. After a fast and simple MRI scout imaging sequence, a PET scan was conducted for the whole-body from the skull vertex to mid-thigh, in 5–6 bed positions. MRI was concurrently conducted using the protocol: T1-weighted 3D volumetric interpolated breath-hold examination (VIBE) with Dixon fat saturation (T1-VIBE-DIXON) (3D, transversal, TR 4.07 ms, TE 1.28 ms, flip angle 12°, 72 slices, 3 mm slice thickness, field of view (FOV) 400 × 400, voxel size 1.3 × 1.3 × 3.0 mm^3), T2W-BLADE (transversal, TR 3000 ms, TE 89 ms, flip angle 90°, 33 slices, Slice thickness 6 mm, FOV 400 × 400, voxel size 1.3 × 1.3 × 6.0 mm^3), DWI (2D, transversal, TR 6270 ms, TE 50 ms, 33 slices, 6 mm slice thickness, FOV 400 × 400, voxel size 1.6 × 1.6 × 6.0 mm^3, b-values 50, 800 s/mm^2). The PET data were reconstructed using high-definition PET (HD-PET) (3 iterations, 21 subsets; matrix 172×172, voxel size 2.3 × 2.3 × 5.0 mm^3). The DIXON sequence was used to derive MRI-based attenuation correction.

^{18}F-FDG PET/CT imaging

Prior to ^{18}F-FDG PET/CT scan, study participants were asked to fast for at least 6 h, ensuring the blood glucose (BG) less than 11.1 mmol/L, and then they were intravenously administered ^{18}F-FDG (3.70–5.55 MBq/kg). All acquisitions were performed on a Biograph 64 PET/CT scanner (Siemens Healthcare, Erlangen, Germany) 45–60 min after ^{18}F-FDG injection. The whole-body CT scanning parameters were set as follows: current (170 mA), voltage (120 kV), and scan layer thickness (3 mm). The PET scan was performed after CT scan acquisition. It was conducted in 5–6 bed positions. Per bed position, PET data were acquired with 2–3 min of acquisition time. Reconstruction of the acquired data was done by the postprocessing workstation with iterative TrueD reconstruction System (Siemens Medical Solutions), and correction attenuation was done by CT images.

Image interpretation

All reconstructed PET/MR as well as PET/CT images were evaluated using Syngo.Via (Siemens Healthcare, Erlangen, Germany) by 2 experienced nuclear medicine physicians. Any difference between the two was solved by consensus.

Pancreatic masses were the target lesions. For lesions with an unclear boundary, contrast-enhanced CT or MR images were referenced during the segmentation. To calculate the standard uptake values (SUVs), circular regions of interest were drawn around the lesions and automatically adapted to a tridimensional volume of interest. For every lesion, the maximum SUV (SUV_{max}), mean SUV (SUV_{mean}) as well as peak SUV (SUV_{peak}) were determined. SUV_{peak} was the SUV_{mean} of a sphere sized 1-cm^3 around the SUV_{max} in the target lesion. As a normal tissue reference, two circular regions of interest (ROIs) with the diameter of 2-cm were drawn in the right and left liver lobe. The averaged SUV_{mean} of each ROI was used as the liver SUV_{mean}. Calculation of tumor-to-liver ratio (TLR) was as: SUV_{max} of the tumor/SUV_{mean} of liver.

If ^{68}Ga-FAPI or ^{18}F-FDG uptake surpassed the surrounding tissue, it was considered a positive lymph node. Distant metastases were assessed by tracer uptake as well as abnormalities in MR signal intensities. Locations of metastases were documented.

Statistical analysis

Data analyses were conducted using SPSS (version 26.0; IBM, Armonk, NY, USA). The quantitative data are presented as mean ± SD. The Wilcoxon signed-rank test was used to compare the number of primary as well as metastatic lesions, respectively identified by two examinations. We used a paired t-test to compare different paired ^{18}F-FDG and ^{68}Ga-FAPI PET SUV parameters. Correlation between ^{68}Ga-FAPI with ^{18}F-FDG SUVs was assessed by Pearson correlation test. $p < 0.05$ was the cutoff for significance, and all tests were two-sided.

Results

Patient characteristics

We recruited 31 patients between January 2020 and July 2021. Patient information including clinical presentation and laboratory indexes was recorded, as summarized in Table 1.

Table 1
Clinical characteristics of all patients

	Pancreatic cancer (n = 28)	**Pancreatitis (n = 3)**
Population		
Age (range, mean)	48–81, 62.82	47–52, 49.33
Gender (M: F)	15:13	2:1
Laboratory		
CA19-9 (> 37U/ml)	20(71.43%)	1(33.33%)
CEA (> 5ng/ml)	9(32.14%)	2(66.67)
CA125(> 35 U/ml)	15(53.57%)	1(33.33%)
History		
Smoking	7(25.00%)	1(33.33%)
Alcohol	6(21.43%)	1(33.33%)
Diabetes	5(17.86%)	1(33.33%)
Hypertension	14(50.00%)	0
Abdominal pain	23(82.14%)	1(33.33%)
Jaundice	4(14.29%)	1(33.33%)
Weight loss	14(50.00%)	1(33.33%)
Treatment		
surgical resection	9(32.14%)	2(66.67%)
EUS-FNA	19(67.86%)	1(33.33%)

Abbreviation: *CA19-9*, carbohydrate antigen 19 − 9; *CEA*, carcinoembryonic antigen; *CA125*, carbohydrate antigen 125; *EUS-FNA*, Endoscopic ultrasound-fine needle aspiration

Clinical diagnosis of suspicious patients

Among the 31 patients, 28 cases were confirmed as pancreatic cancer by pathological results, with 9 patients undergoing surgical resection and 19 patients undergoing endoscopic ultrasound-fine needle aspiration (EUS-FNA). Of the nine surgical samples, eight were pancreatic ductal adenocarcinoma and one was pancreatic adenosquamous carcinoma.

The other three patients were confirmed as pancreatitis. Two were confirmed as chronic pancreatitis by surgery. In the other patient, tumor cells were not detected by needle biopsy, and her clinical symptoms got better after glucocorticoid treatment, the diagnosis of autoimmune pancreatitis was established.

Primary tumor detection

^{18}F-FDG and ^{68}Ga-FAPI PET exhibited comparable detection abilities for primary pancreatic tumors with a 100% positive detection rate. In the primary tumor, uptake parameters of ^{68}Ga-FAPI were higher compared to those of ^{18}F-FDG and the differences were statistically significant ($p < 0.01$, Table 2). We explored the association between uptake of the two tracers. There was no relationship between ^{68}Ga-FAPI and ^{18}F-FDG in SUV_{max}, SUV_{mean} and SUV_{peak} ($p > 0.05$). The TLR of ^{68}Ga-FAPI was moderately correlated to that of ^{18}F-FDG ($r = 0.426$, $p = 0.024$, Fig. 1).

Table 2
Comparison of the primary tumor, lymph node and metastases uptake between ^{68}Ga-FAPI and ^{18}F-FDG PET

		^{68}Ga-FAPI	^{18}F-FDG	t	*p* value
Primary tumor (n = 28)					
	SUV_{max}	12.58 ± 4.58	8.78 ± 3.93	-3.165	0.004
	SUV_{mean}	7.07 ± 2.69	5.00 ± 2.38	-2.930	0.007
	SUV_{peak}	9.59 ± 3.72	6.65 ± 2.99	-3.206	0.003
	TLR	4.24 ± 2.12	3.10 ± 1.50	-2.985	0.006
Lymph node (n = 26)					
	SUV_{max}	9.01 ± 5.14	7.98 ± 3.77	-0.748	0.462
Liver metastases (n = 30)					
	SUV_{max}	6.13 ± 1.63	8.09 ± 1.68	6.079	< 0.001

Elevated tracer uptake was observed in the adjacent tissue of the pancreas at the same time in ^{68}Ga-FAPI imaging in 15 patients (53.57%), which may mask the tumor uptake. The diffused or focal parenchymal uptake in ^{18}F-FDG PET imaging was only observed in 3 patients (10.71% vs. 53.57%, $p < 0.001$). The

SUV_{max} of inflammatory pancreatic parenchyma was higher than that of pancreatic cancer lesions in ^{68}Ga-FAPI (SUV_{max}, 13.76 ± 5.50 *vs.* 12.58 ± 4.58, $p = 0.628$). Two of the 15 patients had a clinical history of chronic pancreatitis and seven showed dilated pancreatic ducts on MR or CT images. Typical cases are presented in Fig. 2 and Fig. 3.

Regional lymph node assessment

In this study, each lymph node with obvious ^{68}Ga-FAPI or ^{18}F-FDG uptake was deemed a positive lymph node. Among the 11 patients with alleged metastasis of lymph nodes, ^{68}Ga-FAPI PET led to N upstaging in 27.27% (3/11) of patients compared with ^{18}F-FDG, upstaging from N0 to N1 occurred in two cases (18.18%) and one (9.09%) from N1 upstaging to N2. However, the difference in lesion numbers detected by ^{68}Ga-FAPI and ^{18}F-FDG PET were not significant (31 *vs.* 26, $p = 0.053$). All ^{18}F-FDG-positive lymph nodes were ^{68}Ga-FAPI positive as well. Typical cases are presented in Fig. 4.

All 26 double-positive lymph nodes exhibited elevated ^{68}Ga-FAPI uptake compared to ^{18}F-FDG, but the difference was insignificant (SUV_{max}, 9.01 ± 5.14 *vs.* 7.98 ± 3.77, $p = 0.462$). No correlation between the two tracers regarding lymph nodal uptake was found ($r = -0.222$, $p = 0.276$).

Distant metastases

Of the three patients with multiple liver metastases, ^{18}F-FDG imaging demonstrated more metastatic lesions than ^{68}Ga-FAPI imaging. ^{18}F-FDG exhibited a higher uptake than ^{68}Ga-FAPI (SUV_{max}, 6.13 ± 1.63 *vs.* 8.09 ± 1.68, $p < 0.001$) in all 30 double-positive intrahepatic metastasis lesions. In these three patients, visual analysis revealed that intrahepatic metastases larger lesions often showed ring-shaped ^{68}Ga-FAPI uptake with tracer merely around the edge of the lesions, and the uptake intensity was significantly lower than those of ^{18}F-FDG. Typical cases are presented in Fig. 5.

All intrahepatic metastases with increased ^{18}F-FDG or ^{68}Ga-FAPI uptake were detected by MRI, and more micrometastases were detected by MRI. However, the results have no influence on tumor M staging, which was important for clinical management and outcomes.

Discussion

The present study was designed as a single-center and prospective study. We compared the diagnosing and staging efficacy of ^{68}Ga-FAPI PET/MR with ^{18}F-FDG PET/CT for pancreatic cancer.

Pancreatic cancer is characterized by vascular deficiency and plentiful desmoplastic stroma, accounting for 90% of the tumor volume. The stroma consists of extracellular matrix proteins and CAFs [20]. Our study revealed that the primary tumor could be visualized by ^{68}Ga-FAPI, which was consistent to previous studies [16,18]. Fibrosis of the pancreas is often a striking feature of chronic pancreatitis [21]. ^{68}Ga-FAPI was not highly tumor-precise than ^{18}F-FDG, and has a limitation of false-positive uptake caused by the

inflammation-induced fibrosis, which has been demonstrated by previous studies [18,[22]]. In this study, there seemed to be an overlap of the uptake intensities in the pancreatic mass and obstructive pancreatitis of pancreatic parenchyma, and it is crucial to differentiate pathological FAPI uptake from tumor-induced obstructive pancreatitis. The positive FAPI uptake caused by tumor-induced inflammation sometimes affects the visual interpretation of PET, thus the qualitative reading of FAPI PET images sometimes must combine other radiological data. Based on the above factors, we suggest to be cautious about the use of ^{68}Ga-FAPI-chelated therapeutic nuclides for intratumoral irradiation treatment for pancreatic cancer, before resolving the hyperconcentration of ^{68}Ga-FAPI in inflammatory pancreatic parenchyma.

Our results indicate that ^{68}Ga-FAPI might be better than ^{18}F-FDG in assessment of lymph node metastasis in pancreatic cancer. Overall, N upstaging occurred in three patients compared with ^{18}F-FDG PET. This result was accordant with previous research [[23]]. These findings may have a significant impact on clinical management. Of course, our disadvantage is that there is no pathological confirmation. A recent study by Qin et al. proposed contrary opinion, who found that the number of avid lymph nodes detected by ^{18}F-FDG was higher than that of ^{68}Ga-FAPI in nasopharyngeal carcinoma (100 *vs.* 48) [[24]]. As we know, ^{18}F-FDG is not tumor-specific, and false-positive results can be found, especially in the inflammatory lesions [6,7]. At the same time, ^{18}F-FDG PET sensitivity may be decreased in metastatic nodes because of low glucose transporter-1 expression, which results in reduced FDG uptake. Therefore, there still exist practical challenges in lymph node staging based on preoperative FDG PET due to above mentioned reasons [6,[25]]. Earlier data show that CAFs can be found in lesions above 1–2 mm in diameter [[26]]. These findings, unfortunately, were not histopathologically verified. Further studies with larger sample size and histopathological results are required to compare the diagnostic accuracy of lymph node metastases between ^{68}Ga-FAPI and ^{18}F-FDG PET in patients of pancreatic cancer.

In our study, the ^{68}Ga-FAPI uptake was usually observed only at the edge of larger lesions of liver metastases. This phenomenon needs further observation and its mechanism need deep study. We speculate that this tracer uptake pattern may be partially attributed to inadequate delivery of the radiotracer to the central portion of the metastatic tumors. Varasteh et al. found that ^{68}Ga-FAPI accumulated predominantly in the border region of permanent coronary artery occlusion [[27]]. The interface of the tumor and the host stroma at the tumor margin is called “the invasive front”. The stroma at the invasive front of the tumor is composed of fibroblasts, myofibroblasts, and myeloid progenitor cells, which are significantly stiffer than those at the tumor core or in normal tissue [[28],[29]]. Tumors composed of more than one component might contribute to intratumoral heterogeneity [[30]]. A previous study also showed that there are three subtypes of CAFs in PDAC [[31]]. We speculate that the above factors may be partly responsible for this phenomenon, and, further studies were needed to explain this phenomenon.

^{18}F-FDG PET/CT, which has a good accuracy, is a powerful screening tool for metastatic disease assessment. However, assessment of liver lesions is inhibited by high background liver uptake as well as other intrinsic technical limitations [32]. In contrast, ^{68}Ga-FAPI demonstrates very low unspecific liver uptake and is expected to be superior for identifying liver metastasis. However, in three patients with liver metastasis in our cases, some ^{18}F-FDG hypermetabolic micrometastases were not detected by ^{68}Ga-FAPI, and the SUV_{max} was significantly lower in ^{68}Ga-FAPI than in ^{18}F-FDG PET. This is contrary to previously published studies that showed ^{68}Ga-FAPI PET/CT identified more metastatic sites than ^{18}F-FDG with a significantly higher SUV [16,23]. The reason for this discrepancy remains unclear, but might be due to the difference in the origins of CAFs. The differences of progenitor cellular origins result in different phenotypes and functions of CAFs [33,34]. Patients who were identified with pancreatic cancer as their only tumor or first primary tumor were included in this study, whereas the metastases reported in other studies consisted of mixed primary tumor compositions, with few pancreatic primary tumors. As mentioned above, MRI has a much higher soft tissue resolution, and the detection rate of lesions is not lower than ^{18}F-FDG [3,6,8,35]. To some extent, integrated PET/MR has made up for the deficiency of low detection rate of ^{68}Ga-FAPI imaging, thus, PET/MR might work as the best partner of ^{68}Ga-FAPI in hepatic metastases. Studies with randomized controlled designs and larger sample sizes should be conducted to verify the difference of ^{68}Ga-FAPI uptake between this study and previous ones.

The lack of a significant correlation between ^{68}Ga-FAPI and ^{18}F-FDG uptake reveals that the two PET tracers provide different information. ^{18}F-FDG is a glucose analog, thus its uptake reflects glucose uptake and, indirectly, metabolic activity [4]. ^{68}Ga-FAPI is a ligand based on quinoline targeting cancer-associated fibroblasts [16]. Qin et al. also did not find any correlation in tumor uptake values of the two tracers [24].

As a result of the small sample size, we focused on comparative study of ^{18}F-FDG imaging as well as ^{68}Ga-FAPI imaging in pancreatic cancer, as well as the preliminary study of the additional value of PET/MR. The comparative study of MRI and PET-related parameters will be discussed in the subsequent article of this series.

Conclusion

^{68}Ga-FAPI did not show overwhelming superiority to ^{18}F-FDG in visualizing the primary pancreatic cancer. ^{68}Ga-FAPI might be better than ^{18}F-FDG in lymph node metastasis, but the value of ^{68}Ga-FAPI PET for N staging need further study. The characteristics of ^{68}Ga-FAPI uptake in intrahepatic metastases require larger sample size studies for corroboration. The MRI multiple sequence imaging of integrated PET/MR has many advantages and was helpful for detecting tiny liver metastases, thus we recommend the use of PET/MR for ^{68}Ga-FAPI imaging for pancreatic cancer diagnosing and staging.

Declarations

Funding

We gratefully acknowledge the financial supports by the National Natural Science Foundation of China (Grant No. 82001867, and 81871390), and the “234 Discipline Climbing Plan” of the First Affiliated Hospital of Naval Medical University (Grant No. 2019YPT002, and 2020YPT002).

Availability of data and material

Not applicable.

Code availability

Not applicable.

Ethics approval

This article does not contain any studies with animals. All procedures of this study followed the Declaration of Helsinki principles. This prospective study was approved by the Ethics Committee of the First Affiliated Hospital of Naval Medical University (Changhai Hospital, CHEC2021-071).

Consent to participate

All subjects provided written informed consent.

Consent for publication

Informed consent was obtained from all individual participants included in this study.

Conflict of interest

The authors declare that they have no conflict of interest.

Authors’ contributions

Zeyu Zhang, Guorong Jia, Chao Cheng and Changjing Zuo designed the study, interpreted the data, and led the writing and review of the manuscript. Kai Cao, Guixia Pan and Lu Zhang synthesised the ^{68}Ga-FAPI-04 and performed the examination. Zeyu Zhang, Guorong Jia, Qinqin Yang, Hongyu Meng and Jian Yang collected clinical and imaging data. Chao Cheng and Changjing Zuo participated in the review of the manuscript.

References

1. Siegel RL, Miller KD, Jemal A. Cancer statistics, 2020. CA Cancer J Clin. 2020;70:7–30. https://doi.org/10.3322/caac.21590.
2. Kleeff J, Korc M, Apte M, La Vecchia C, Johnson CD, Biankin AV, et al. Pancreatic cancer. Nat Rev Dis Primers. 2016;2:16022. https://doi.org/10.1038/nrdp.2016.22.

3. Yeh R, Dercle L, Garg I, Wang ZJ, Hough DM, Goenka AH. The Role of 18F-FDG PET/CT and PET/MRI in Pancreatic Ductal Adenocarcinoma. Abdom Radiol (NY). 2018;43:415–34. https://doi.org/10.1007/s00261-017-1374-2.
4. Lee JW, O JH, Choi M, Choi JY. Impact of F-18 Fluorodeoxyglucose PET/CT and PET/MRI on Initial Staging and Changes in Management of Pancreatic Ductal Adenocarcinoma: A Systemic Review and Meta-Analysis. Diagnostics (Basel). 2020;10:952. https://doi.org/10.3390/diagnostics10110952.
5. Wang L, Dong P, Shen G, Hou S, Zhang Y, Liu X, Tian B. 18F-Fluorodeoxyglucose Positron Emission Tomography Predicts Treatment Efficacy and Clinical Outcome for Patients With Pancreatic Carcinoma: A Meta-analysis. Pancreas. 2019;48:996–1002. https://doi.org/10.1097/MPA.0000000000001375.
6. Rijkers AP, Valkema R, Duivenvoorden HJ, van Eijck CH. Usefulness of F-18-fluorodeoxyglucose positron emission tomography to confirm suspected pancreatic cancer: a meta-analysis. Eur J Surg Oncol. 2014;40:794–804. https://doi.org/10.1016/j.ejso.2014.03.016.
7. Strobel O, Büchler MW. Pancreatic cancer: FDG-PET is not useful in early pancreatic cancer diagnosis. Nat Rev Gastroenterol Hepatol. 2013;10:203–5. https://doi.org/10.1038/nrgastro.2013.42.
8. Sagiyama K, Watanabe Y, Kamei R, Hong S, Kawanami S, Matsumoto Y, et al. Multiparametric voxel-based analyses of standardized uptake values and apparent diffusion coefficients of soft-tissue tumours with a positron emission tomography/magnetic resonance system: Preliminary results. Eur Radiol. 2017;27:5024–33. https://doi.org/10.1007/s00330-017-4912-y.
9. Erkan M, Hausmann S, Michalski CW, Fingerle AA, Dobritz M, Kleeff J, et al. The role of stroma in pancreatic cancer: diagnostic and therapeutic implications. Nat Rev Gastroenterol Hepatol. 2012;9:454–67. https://doi.org/10.1038/nrgastro.2012.115.
10. Nielsen MFB, Mortensen MB, Detlefsen S. Typing of pancreatic cancer-associated fibroblasts identifies different subpopulations. World J Gastroenterol. 2018;24:4663–78. https://doi.org/10.3748/wjg.v24.i41.4663.
11. Whittle MC, Hingorani SR. Fibroblasts in Pancreatic Ductal Adenocarcinoma: Biological Mechanisms and Therapeutic Targets. Gastroenterology. 2019;156:2085–96. https://doi.org/10.1053/j.gastro.2018.12.044.
12. Piersma B, Hayward MK, Weaver VM. Fibrosis and cancer: A strained relationship. Biochim Biophys Acta Rev Cancer. 2020;1873:188356. https://doi.org/10.1016/j.bbcan.2020.188356.
13. von Ahrens D, Bhagat TD, Nagrath D, Maitra A, Verma A. The role of stromal cancer-associated fibroblasts in pancreatic cancer. J Hematol Oncol. 2017;10:76. https://doi.org/10.1186/s13045-017-0448-5.
14. Mikuła-Pietrasik J, Uruski P, Tykarski A, Książek K. The peritoneal "soil" for a cancerous "seed": a comprehensive review of the pathogenesis of intraperitoneal cancer metastases. Cell Mol Life Sci. 2018;75:509–25. https://doi.org/10.1007/s00018-017-2663-1.

15. Yang X, Lin Y, Shi Y, Li B, Liu W, Yin W, Dang Y, Chu Y, Fan J, He R. FAP Promotes Immunosuppression by Cancer-Associated Fibroblasts in the Tumor Microenvironment via STAT3-CCL2 Signaling. Cancer Res. 2016;76:4124–35. https://doi.org/10.1158/0008-5472.CAN-15-2973.
16. Kratochwil C, Flechsig P, Lindner T, Abderrahim L, Altmann A, Mier W, et al. 68Ga-FAPI PET/CT: Tracer Uptake in 28 Different Kinds of Cancer. J Nucl Med. 2019;60:801–5. https://doi.org/10.2967/jnumed.119.227967.
17. Giesel FL, Kratochwil C, Lindner T, Marschalek MM, Loktev A, Lehnert W, et al. 68Ga-FAPI PET/CT: Biodistribution and Preliminary Dosimetry Estimate of 2 DOTA-Containing FAP-Targeting Agents in Patients with Various Cancers. J Nucl Med. 2019;60:386–92. https://doi.org/10.2967/jnumed.118.215913.
18. Röhrich M, Naumann P, Giesel FL, Choyke PL, Staudinger F, Wefers A, et al. Impact of 68Ga-FAPI PET/CT Imaging on the Therapeutic Management of Primary and Recurrent Pancreatic Ductal Adenocarcinomas. J Nucl Med. 2021;62:779–86. https://doi.org/10.2967/jnumed.120.253062.
19. Lindner T, Loktev A, Altmann A, et al. Development of Quinoline-Based Theranostic Ligands for the Targeting of Fibroblast Activation Protein. J Nucl Med. 2018;59:1415–22. https://doi.org/10.2967/jnumed.118.210443.
20. González-Borja I, Viúdez A, Goñi S, Santamaria E, Carrasco-García E, Pérez-Sanz J, et al. Omics Approaches in Pancreatic Adenocarcinoma. Cancers (Basel). 2019;11:1052. https://doi.org/10.3390/cancers11081052.
21. Kleeff J, Whitcomb DC, Shimosegawa T, Esposito I, Lerch MM, Gress T, et al. Chronic pancreatitis. Nat Rev Dis Primers. 2017;3:17060. https://doi.org/10.1038/nrdp.2017.60.
22. Luo Y, Pan Q, Yang H, Peng L, Zhang W, Li F. Fibroblast Activation Protein-Targeted PET/CT with 68Ga-FAPI for Imaging IgG4-Related Disease: Comparison to 18F-FDG PET/CT. J Nucl Med. 2021;62:266–71. https://doi.org/10.2967/jnumed.120.244723.
23. Chen H, Pang Y, Wu J, et al. Comparison of [68Ga]Ga-DOTA-FAPI-04 and [18F] FDG PET/CT for the diagnosis of primary and metastatic lesions in patients with various types of cancer. Eur J Nucl Med Mol Imaging. 2020;47:1820–32. https://doi.org/10.1007/s00259-020-04769-z.
24. Qin C, Liu F, Huang J, Ruan W, et al. A head-to-head comparison of 68Ga-DOTA-FAPI-04 and 18F-FDG PET/MR in patients with nasopharyngeal carcinoma: a prospective study. Eur J Nucl Med Mol Imaging. 2021;48:3228–37. https://doi.org/10.1007/s00259-021-05255-w.
25. Mallak N, Hope TA, Guimaraes AR. PET/MR Imaging of the Pancreas. Magn Reson Imaging Clin N Am. 2018;26:345–62. https://doi.org/10.1016/j.mric.2018.03.003.
26. Davidson B, Goldberg I, Kopolovic J. Inflammatory response in cervical intraepithelial neoplasia and squamous cell carcinoma of the uterine cervix. Pathol Res Pract. 1997;193:491–5. https://doi.org/10.1016/s0344-0338(97)80102-1.
27. Varasteh Z, Mohanta S, Robu S, Braeuer M, Li Y, Omidvari N, et al. Molecular Imaging of Fibroblast Activity After Myocardial Infarction Using a 68Ga-Labeled Fibroblast Activation Protein Inhibitor, FAPI-04. J Nucl Med. 2019;60:1743–9. https://doi.org/10.2967/jnumed.119.226993.

28. Acerbi I, Cassereau L, Dean I, Shi Q, Au A, Park C, et al. Human breast cancer invasion and aggression correlates with ECM stiffening and immune cell infiltration. Integr Biol (Camb). 2015;7:1120–34. https://doi.org/10.1039/c5ib00040h.
29. Clark AG, Vignjevic DM. Modes of cancer cell invasion and the role of the microenvironment. Curr Opin Cell Biol. 2015;36:13–22. https://doi.org/10.1016/j.ceb.2015.06.004.
30. Ribeiro IP, Melo JB, Carreira IM. Cytogenetics and Cytogenomics Evaluation in Cancer. Int J Mol Sci. 2019;20:4711. https://doi.org/10.3390/ijms20194711.
31. Elyada E, Bolisetty M, Laise P, Flynn WF, Courtois ET, Burkhart RA, et al. Cross-Species Single-Cell Analysis of Pancreatic Ductal Adenocarcinoma Reveals Antigen-Presenting Cancer-Associated Fibroblasts. Cancer Discov. 2019;9:1102–23. https://doi.org/10.1158/2159-8290.CD-19-0094.
32. Wang XY, Yang F, Jin C, Fu DL. Utility of PET/CT in diagnosis, staging, assessment of resectability and metabolic response of pancreatic cancer. World J Gastroenterol. 2014;20:15580–9. https://doi.org/10.3748/wjg.v20.i42.15580.
33. Sharon Y, Raz Y, Cohen N, Ben-Shmuel A, Schwartz H, Geiger T, et al. Tumor-derived osteopontin reprograms normal mammary fibroblasts to promote inflammation and tumor growth in breast cancer. Cancer Res. 2015;75:963–73. https://doi.org/10.1158/0008-5472.CAN-14-1990.
34. Neesse A, Bauer CA, Öhlund D, Lauth M, Buchholz M, Michl P, et al. Stromal biology and therapy in pancreatic cancer: ready for clinical translation? Gut. 2019;68:159–71. https://doi.org/10.1136/gutjnl-2018-316451.
35. Chen WS, Li JJ, Hong L, Xing ZB, Wang F, Li CQ. Comparison of MRI, CT and 18F-FDG PET/CT in the diagnosis of local and metastatic of nasopharyngeal carcinomas: an updated meta analysis of clinical studies. Am J Transl Res. 2016;8:4532–47.

Figures

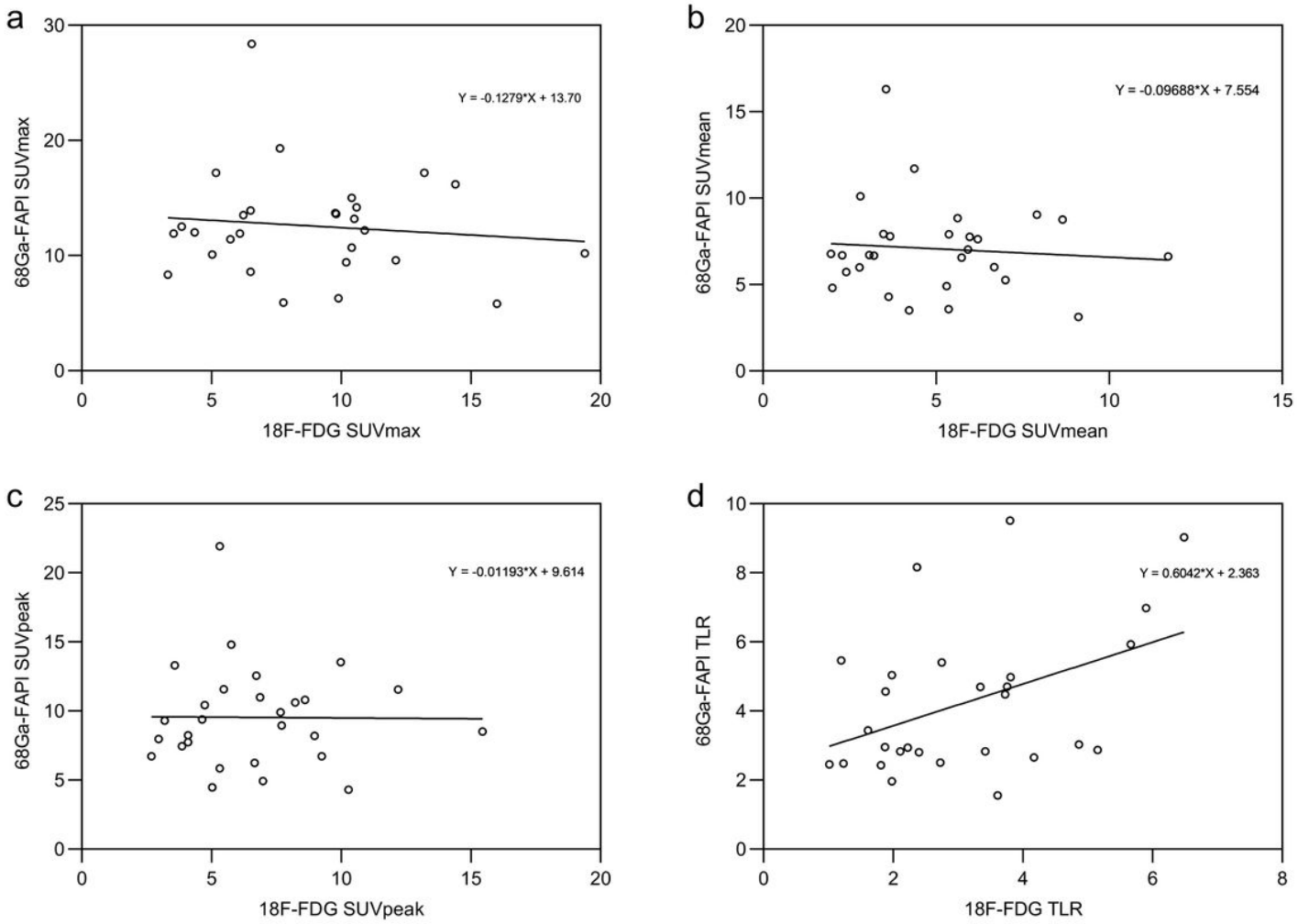

Figure 1

Comparison of SUVmax, SUVmean, SUVpeak and TLR of 68Ga-FAPI with 18F-FDG in primary tumor. The SUVmax, SUVmean, and SUVpeak measured with 68Ga-FAPI as well as 18F-FDG were not significantly correlated ($p > 0.05$). The TLR of 68Ga-FAPI was mildly moderately correlated with 18F-FDG ($r = 0.426$, $p = 0.024$)

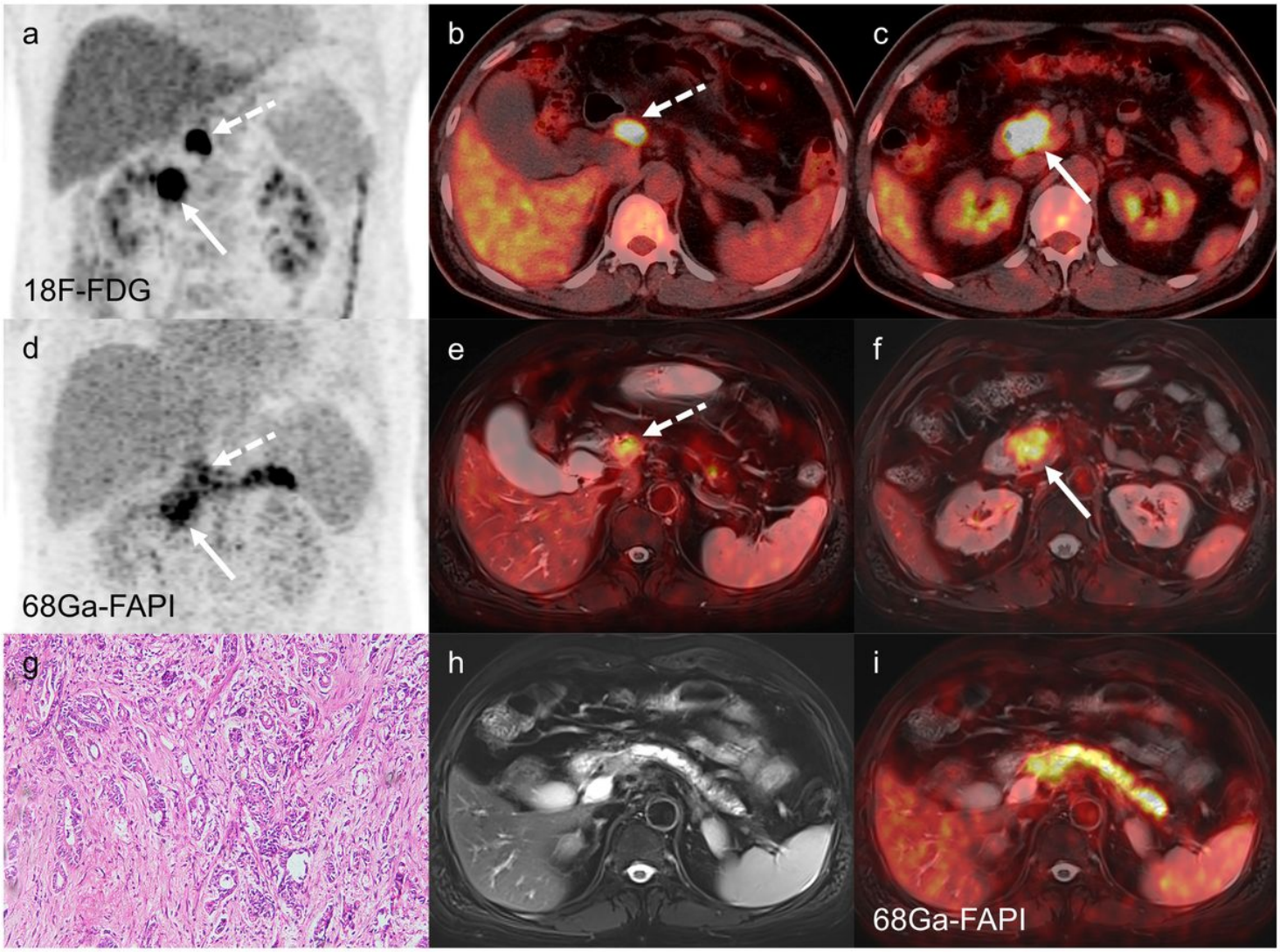

Figure 2

A man (53-year-old) with a pancreatic ductal adenocarcinoma (PDAC). (a-f) 68Ga-FAPI PET/MR and 18F-FDG PET/CT exhibited a high focal uptake (FAPI: SUVmax = 9.59; FDG: SUVmax = 12.10) in the pancreatic head (arrows) and lymph node metastasis (FAPI: SUVmax = 6.77; FDG: SUVmax = 15.40) in the lesser omentum (dashed arrows). (g) Hematoxylin-eosin (HE) staining of pancreatic cancer tissues (200× magnification). (h-i) Dilatation of the major pancreatic duct with obstructive pancreatitis related 68Ga-FAPI uptake in the region of body and pancreatic tail (SUVmax = 11.70)

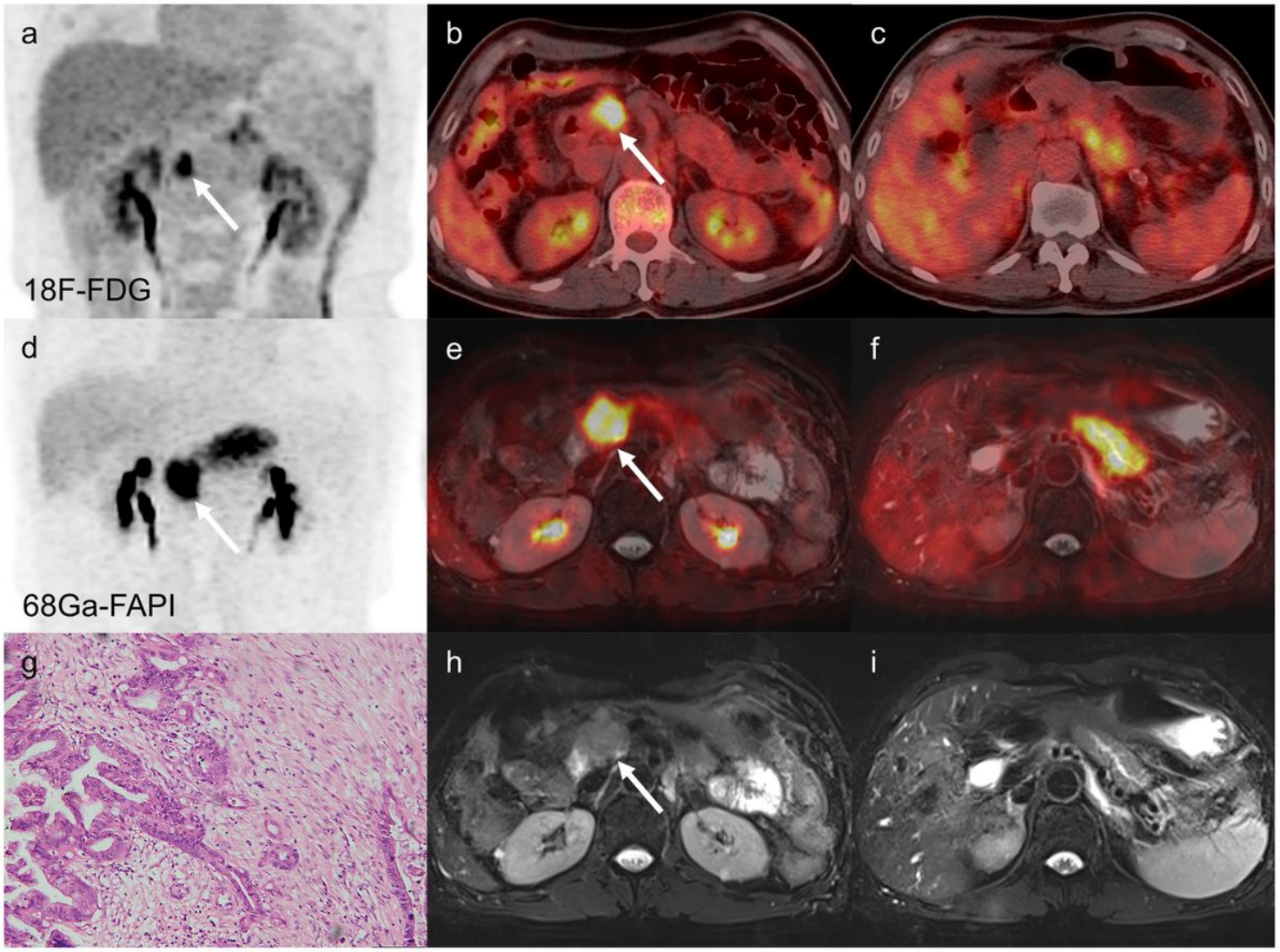

Figure 3

A man (72 years old) with pancreatic ductal adenocarcinoma (PDAC). 68Ga-FAPI PET/MR and 18F-FDG PET/CT exhibited a high focal uptake (FAPI: SUVmax = 19.30; FDG: SUVmax = 7.64) in the pancreatic head (arrows). Pancreatitis related 68Ga-FAPI uptake could be seen in the pancreatic body and tail (SUVmax = 14.9), nodular 18F-FDG uptake could also be seen in the body of pancreas (SUVmax = 4.34)

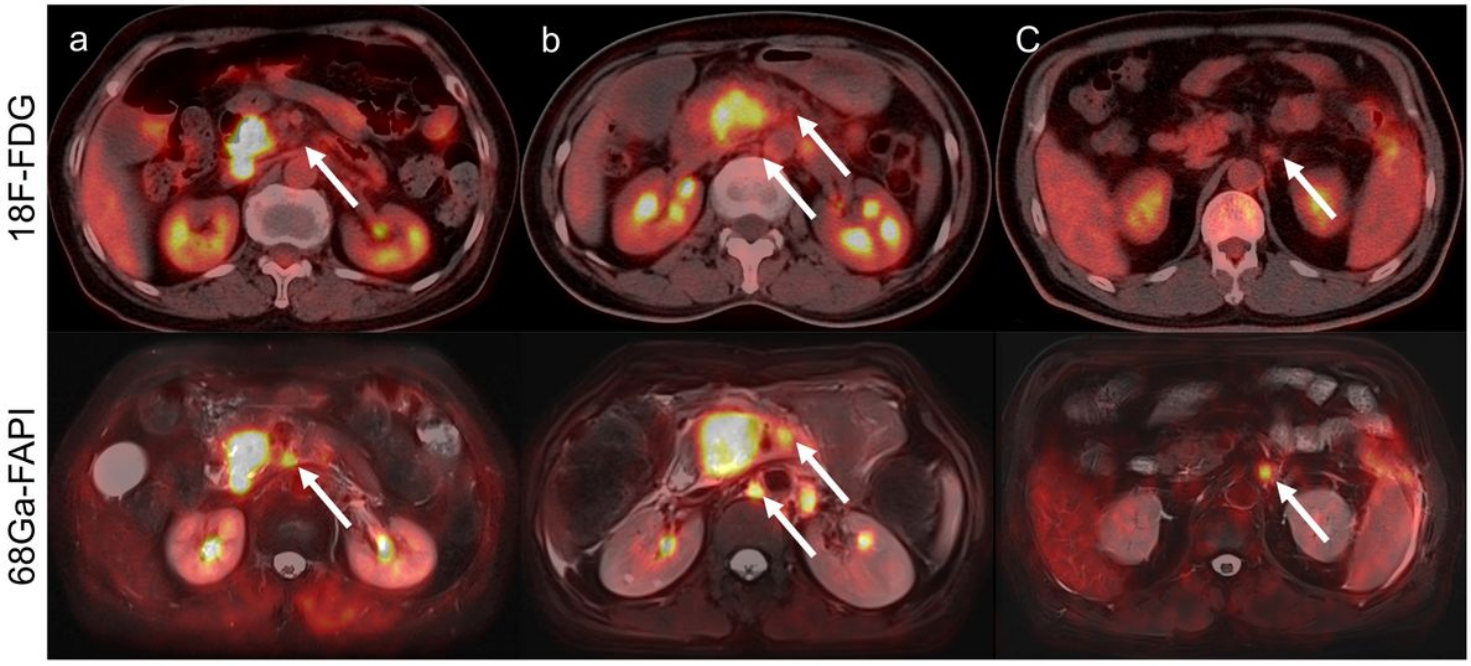

Figure 4

In these three patients, 18F-FDG-negative lymph nodes were showed 68Ga-FAPI-positive (arrows)

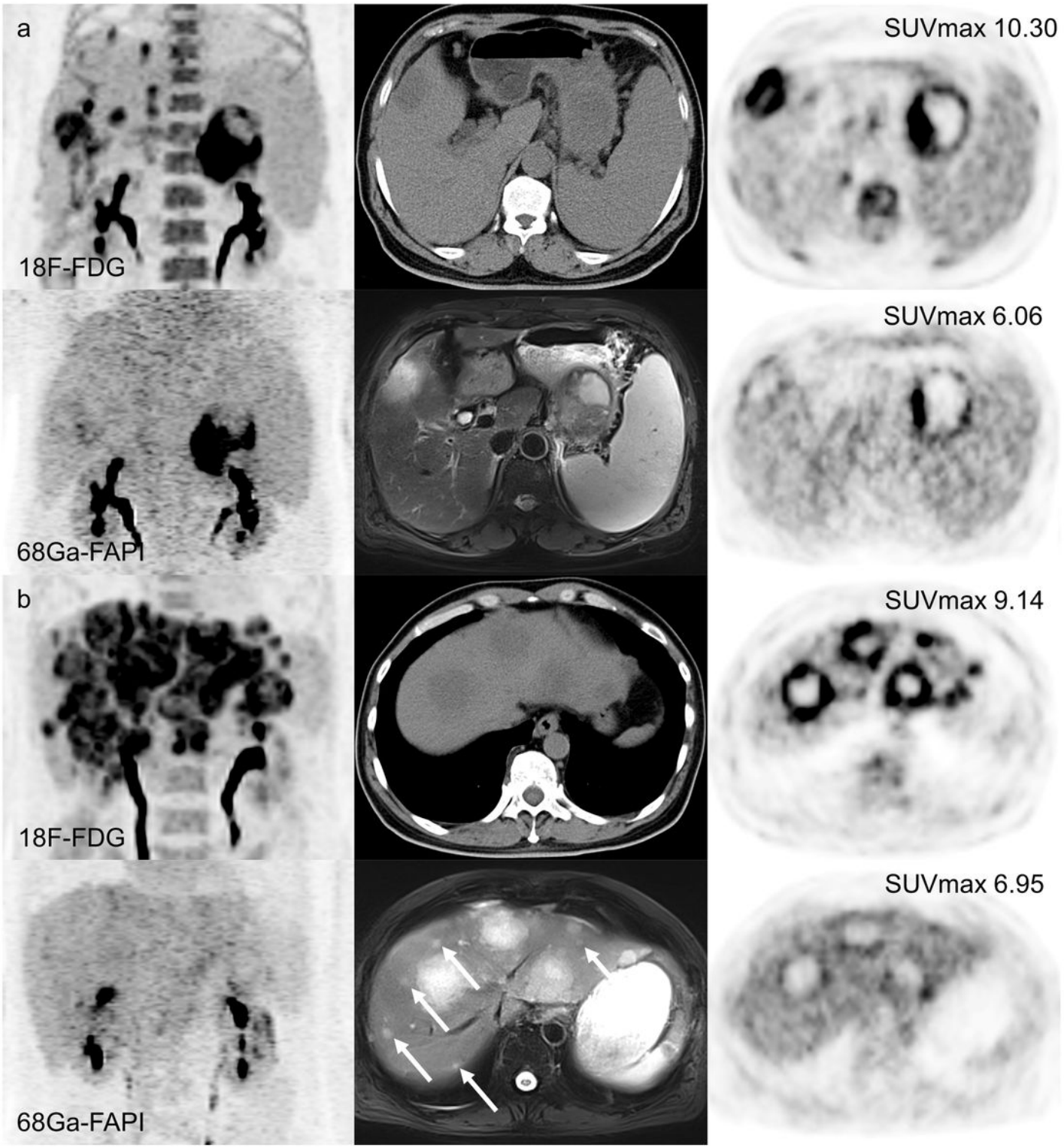

Figure 5

Two liver metastatic patients of pancreatic tumor, 68Ga-FAPI uptake was only detected at the edge of liver metastases, and the 18F-FDG uptake intensity was more obvious. All intrahepatic metastases with increased 18F-FDG metabolism were detected by MRI, and more micrometastases undetectable by CT were identified by MRI (arrows)